

Jaroslav Fořt; Jiří Fürst; J. Halama; Karel Kozel

Numerical simulation of 3D transonic flow through cascades

Mathematica Bohemica, Vol. 126 (2001), No. 2, 353–361

Persistent URL: <http://dml.cz/dmlcz/134021>

Terms of use:

© Institute of Mathematics AS CR, 2001

Institute of Mathematics of the Czech Academy of Sciences provides access to digitized documents strictly for personal use. Each copy of any part of this document must contain these *Terms of use*.



This document has been digitized, optimized for electronic delivery and stamped with digital signature within the project *DML-CZ: The Czech Digital Mathematics Library* <http://dml.cz>

NUMERICAL SIMULATION OF 3D TRANSONIC FLOW THROUGH CASCADES

J. FOŘT, J. FÜRST, J. HALAMA, K. KOZEL, Praha

Dedicated to Prof. J. Nečas on the occasion of his 70th birthday

Abstract. The paper deals with the numerical solution of 3D transonic flow through axial turbine cascades. Finite volume methods based on TVD MacCormack cell-centered and Ni's cell-vertex schemes are discussed. A comparison of numerical results for 3D stator and rotor cascades is presented.

Keywords: transonic flow, finite volume methods, Euler equations, turbines

MSC 2000: 76H05, 76M25

1. INTRODUCTION

Numerical simulation of transonic flows in a turbomachinery branch is the subject of our long time cooperation with industry. Several numerical methods for the computation of 2D flow through cascades were developed and some of them have been extended to 3D. All numerical methods have been tested on several test cases. Their results are validated using other numerical results as well as the experimental data.

This work has been supported by the grants No. 201/99/0267 and 101/00/1057 of Grant Agency of Czech Republic and by the Research Project No. J04/98/212200009 of MŠMT ČR.

2. GOVERNING EQUATIONS

The transonic flow through LP (low pressure) turbine cascades at design conditions is characterized by a negligible boundary layer thickness and the dominant role of trailing edge shocks and their reflections. All features mentioned can be modelled using inviscid flow described by the system of Euler equations (1)

$$\begin{aligned}
 (1) \quad & \mathbf{W}_t + \mathbf{F}_x + \mathbf{G}_y + \mathbf{H}_z = \mathbf{Q}, \\
 & \mathbf{W} = [\varrho, \varrho w_1, \varrho w_2, \varrho w_3, e]^T, \\
 & \mathbf{F} = [\varrho w_1, \varrho w_1^2 + p, \varrho w_1 w_2, \varrho w_1 w_3, w_1(e + p)]^T, \\
 & \mathbf{G} = [\varrho w_2, \varrho w_2 w_1, \varrho w_2^2 + p, \varrho w_2 w_3, w_2(e + p)]^T, \\
 & \mathbf{H} = [\varrho w_3, \varrho w_3 w_1, \varrho w_3 w_2, \varrho w_3^2 + p, w_3(e + p)]^T, \\
 & \mathbf{Q} = [0, 0, \varrho(\omega^2 y - 2\omega w_3), \varrho(\omega^2 z + 2\omega w_2), 0]^T.
 \end{aligned}$$

This system of equations is closed by the equation of state for ideal gas:

$$(2) \quad p = (\kappa - 1) \left[e - \varrho \frac{w_1^2 + w_2^2 + w_3^2}{2} + \frac{1}{2} \varrho \omega^2 R^2 \right].$$

The symbol ϱ denotes density, w_i are the Cartesian components of the relative velocity vector, e is the total energy per unit volume, p is the static pressure, ω is the angular velocity, κ is the ratio of specific heats and R is the radius. The right hand side of Eq. (1) is equal to zero for the flow in the absolute frame of reference, i.e. with $\omega = 0$.

3. MATHEMATICAL FORMULATION

The domain of solution Ω consists of one cascade pitch. A solution \mathbf{W} has to fulfill the integral form (3) of Eq. (1) inside any domain $D \subset \Omega$ with sufficiently smooth boundary and boundary conditions along $\partial\Omega$.

$$(3) \quad \int_{t_1}^{t_2} \iiint_D (\mathbf{W}_t + \mathbf{F}_x + \mathbf{G}_y + \mathbf{H}_z - \mathbf{Q}) \, dV \, dt = 0.$$

Four different types of boundary conditions are distinguished. First, the non-permeability condition $\vec{w} \cdot \vec{n} = 0$ (\vec{n} denotes the unit vector perpendicular to the wall) is prescribed along walls (ABCDEFGH is the hub casing, A'B'C'D'E'F'G'H' is the tip casing, BCC'B' and GFF'G' are the blade surfaces). Second, the stagnation values of the density ϱ_0 and the speed of sound a_0 and the radial distribution of the velocity angles c_i are imposed on the inlet section (AHH'A'). Two more parameters

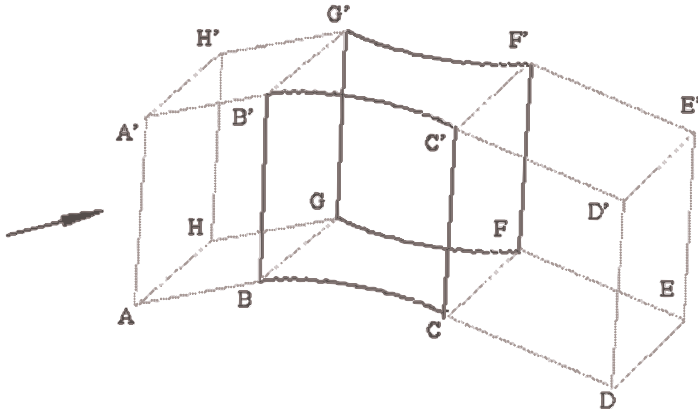


Fig. 1. Computational domain

$\frac{\varrho_{\text{rel},0}}{\varrho_0}$ and $\frac{a_{\text{rel},0}}{a_0}$, which represents the total relative quantities at the rotor inlet divided by the total quantities at the stator inlet, are added at the inlet section in case of a rotor flow. The ratio $\frac{\varrho^d}{\varrho_{\text{rel},0}}$, which is computed from the isentropic relations in the relative frame of reference, premultiplied by $\frac{\varrho_{\text{rel},0}}{\varrho_0}$, gives the ratio $\frac{\varrho^d}{\varrho_0}$, i.e. the non-dimensional density with respect to the chosen reference value ϱ_0 . The same arrangement is used for the velocity components w_i and the energy e ,

$$\varrho = \frac{\varrho^d}{\varrho_0} = \frac{\varrho^d}{\varrho_{\text{rel},0}} \cdot \frac{\varrho_{\text{rel},0}}{\varrho_0},$$

$$w_i = \frac{w_i^d}{a_0} = \frac{w_i^d}{a_{\text{rel},0}} \cdot \frac{a_{\text{rel},0}}{a_0},$$

$$e = \frac{e^d}{\varrho_0 a_0^2} = \frac{e^e}{\varrho_{\text{rel},0} a_{\text{rel},0}^2} \cdot \frac{\varrho_{\text{rel},0} a_{\text{rel},0}^2}{\varrho_0 a_0^2},$$

where the superscript d denotes the physical dimensional quantity. Third, the distribution of the outlet static pressure $p = p(R)$ is given at the outlet (DEE'D') and last, the periodical condition is used along the periodical boundary (ABB'A', CDD'C', FEE'F' and HGG'H').

4. NUMERICAL METHODS

Numerical solution has been computed on a structured hexahedral H-type grid (example is in Fig. 2) by two different methods.

The former, based on the TVD MacCormack cell centered scheme (Causon [2]), is described below by equations (4) representing 1D version in the absolute frame

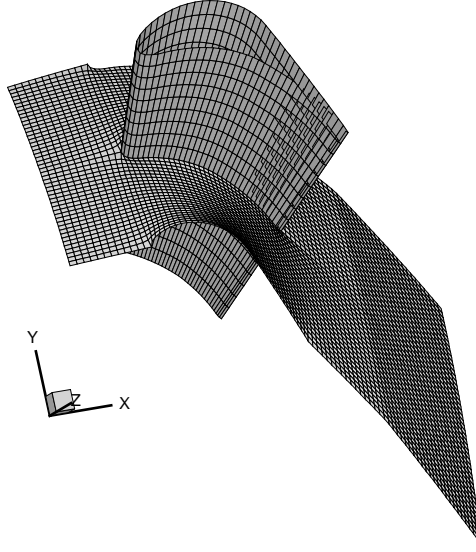


Fig. 2. H-type computational grid

of reference. The first two equations represent the classical predictor and corrector steps while the third is a TVD correction

$$\begin{aligned}
 \mathbf{W}_i^{n+\frac{1}{2}} &= \mathbf{W}_i^n - \frac{\Delta t}{\Delta x} [\mathbf{F}(\mathbf{W}_i^n) - \mathbf{F}(\mathbf{W}_{i-1}^n)], \\
 \overline{\mathbf{W}_i^{n+1}} &= \frac{1}{2} \left(\mathbf{W}_i^n + \mathbf{W}_i^{n+\frac{1}{2}} - \frac{\Delta t}{\Delta x} [\mathbf{F}(\mathbf{W}_{i+1}^{n+\frac{1}{2}}) - \mathbf{F}(\mathbf{W}_i^{n+\frac{1}{2}})] \right), \\
 \mathbf{W}_i^{n+1} &= \overline{\mathbf{W}_i^{n+1}} + (g_i^+ + g_{i+1}^-) (\mathbf{W}_{i+1}^n - \mathbf{W}_i^n) - (g_{i-1}^+ + g_i^-) (\mathbf{W}_i^n - \mathbf{W}_{i-1}^n),
 \end{aligned}
 \tag{4}$$

where

$$\begin{aligned}
 g_i^\pm &= \frac{1}{2} C(\nu) [1 - \Phi(r_i^\pm)], \\
 C(\nu) &= \begin{cases} \nu(1 - \nu) & \nu < 0.5 \\ 0.25 & \nu \geq 0.5 \end{cases} \\
 \nu &= \frac{\Delta t}{\Delta x} \varrho_A = \frac{\Delta t}{\Delta x} (|u| + a), \quad a^2 = \kappa \frac{p}{\varrho}, \\
 r_i^\pm &= (\Delta W_{i-\frac{1}{2}}, \Delta W_{i+\frac{1}{2}}) / \|\Delta W_{i\pm\frac{1}{2}}\|^2, \\
 \Phi(r) &= \min\text{mod}(2r, 1) = \max[0, \min(2r, 1)],
 \end{aligned}$$

where i , j and k are grid indexes in streamwise, pitchwise and spanwise directions respectively, n denotes the time index. The modification, where ν is computed using the smallest absolute value of the eigenvalue instead of the spectral radius ϱ_A , contains a lower amount of artificial viscosity, see [3].

The latter, based on the Ni's cell-vertex scheme (Ni [1]), approximates the following integral relation (5)

(5)

$$\begin{aligned} \mathbf{W}_{ijk}^{n+1} - \mathbf{W}_{ijk}^n &= -\Delta t \sum_{m=1}^8 \frac{\mu(V_m)}{\mu(D)} \frac{1}{\mu(V_m)} \oint \oint_{\partial V_m} (\mathbf{F}, \mathbf{G}, \mathbf{H}) \mathbf{n} dS \\ &+ \frac{\Delta t^2}{2\mu(\tilde{D})} \oint \oint_{\partial \tilde{D}} (\mathbf{F}_{\mathbf{W}} \operatorname{div}(\mathbf{F}, \mathbf{G}, \mathbf{H}), \mathbf{G}_{\mathbf{W}} \operatorname{div}(\mathbf{F}, \mathbf{G}, \mathbf{H}), \mathbf{H}_{\mathbf{W}} \operatorname{div}(\mathbf{F}, \mathbf{G}, \mathbf{H})) \mathbf{n} dS \\ &+ \frac{\Delta t}{\mu(D)} \iiint_{\mathbf{Q}} dV + \frac{\Delta t^2}{2\mu(\tilde{D})} \iiint_{\tilde{D}} \mathbf{Q}_{\mathbf{W}} \operatorname{div}(\mathbf{F}, \mathbf{G}, \mathbf{H}) dV, \end{aligned}$$

where the first two terms are the first and second order convective terms and the last two terms are the first and second order terms including the body forces. The control volume D consists of eight cells V_m ($m = 1, \dots, 8$) and \tilde{D} is the cell of the dual mesh. The symbol $\mu(D)$ denotes the volume of D . The second order terms on the right hand side of eq. (5) contain Jacobi matrices $\mathbf{F}_{\mathbf{W}} = \frac{\partial \mathbf{F}}{\partial \mathbf{W}}$, etc.

Numerical realization of eq. (5) is shown for 2D case, which is both general enough and easier to follow. Computation of unknowns in a new time level consists of three steps:

1. Computation of cell residuals $R\mathbf{W}$:

$$R\mathbf{W}_{i,j} = \frac{\Delta t}{2\mu_{i,j}} \sum_{m=1}^4 ((\mathbf{F}_m^n + \mathbf{F}_{m+1}^n)\Delta y_m - (\mathbf{G}_m^n + \mathbf{G}_{m+1}^n)\Delta x_m).$$

The residual $R\mathbf{W}$ approximates the first integral on the right hand side of Eq. (5). Besides common grid indexes i and j there is a local index $m = 1, \dots, 4$ inside each cell pointing at vertices, see Fig. 3.

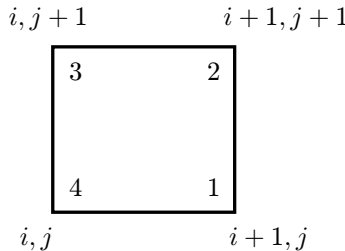


Fig. 3. Grid cell

2. Distribution of cell residuals into vertices:

$$\begin{aligned}
 \delta \mathbf{W}_1 &= -R\mathbf{W}_{i,j} - \mathbf{f} + \mathbf{g} + D_{L_1}, \\
 \delta \mathbf{W}_2 &= -R\mathbf{W}_{i,j} - \mathbf{f} - \mathbf{g} + D_{L_2}, \\
 \delta \mathbf{W}_3 &= -R\mathbf{W}_{i,j} + \mathbf{f} - \mathbf{g} + D_{L_3}, \\
 \delta \mathbf{W}_4 &= -R\mathbf{W}_{i,j} + \mathbf{f} + \mathbf{g} + D_{L_4}, \\
 \mathbf{f} &= (\Delta t / \mu_{i,j}) (\mathbf{F}_W \Delta_y y - \mathbf{G}_W \Delta_x x + \varepsilon_N |\Delta_x \mathbf{W}| \Delta_x \mathbf{W} \Delta t / (2\Delta_x x \mu_{i,j})), \\
 \mathbf{g} &= (\Delta t / \mu_{i,j}) (\mathbf{G}_W \Delta_x x - \mathbf{F}_W \Delta_y y + \varepsilon_N |\Delta_y \mathbf{W}| \Delta_y \mathbf{W} \Delta t / (2\Delta_y y \mu_{i,j})), \\
 D_{L_l} &= \varepsilon_L \left(\frac{\Delta t}{\Delta_x x} + \frac{\Delta t}{\Delta_y y} \right) \left(\sum_{m=1}^4 (\mathbf{W}_m - \mathbf{W}_l) \right),
 \end{aligned}$$

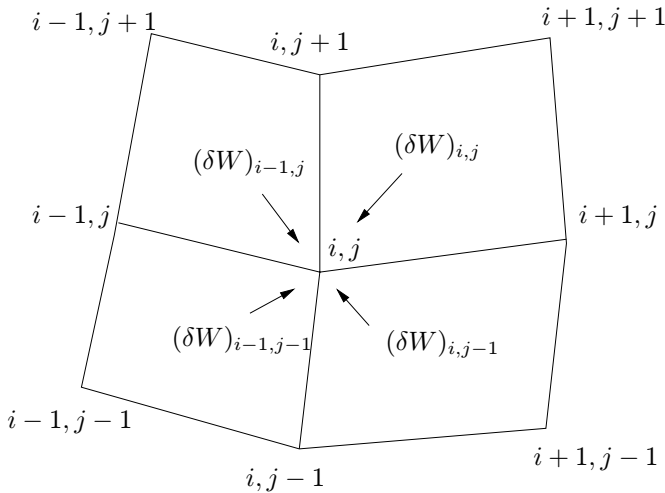
where

$$\Delta_y a = a_2 + a_3 - a_4 - a_1, \quad \Delta_x a = a_2 + a_1 - a_3 - a_4,$$

where μ_{ij} is the volume of a cell, for which the vertex with the local index $m = 1$ has global indexes i and j . User specified coefficients ε_L and ε_N control the amount of artificial viscosity. The terms \mathbf{f} and \mathbf{g} approximate the second integral on the right hand side of Eq. (5).

3. Computation of unknowns \mathbf{W}^{n+1} at cell vertices:

$$\begin{aligned}
 \mathbf{W}_{i,j}^{n+1} &= \mathbf{W}_{i,j}^n + (\mu_{i,j} + \mu_{i-1,j} + \mu_{i-1,j-1} + \mu_{i,j-1})^{-1} \\
 &\quad \times (\mu_{i,j} (\delta \mathbf{W}_4)_{i,j} + \mu_{i-1,j} (\delta \mathbf{W}_1)_{i-1,j} \\
 &\quad + \mu_{i-1,j-1} (\delta \mathbf{W}_2)_{i-1,j-1} + \mu_{i,j-1} (\delta \mathbf{W}_3)_{i,j-1}).
 \end{aligned}$$



5. NUMERICAL RESULTS

Results for two axial cascades of the last LP steam turbine stage of Škoda Turbines, Pilsen are presented in this section. The first cascade is the stator cascade with strong divergence of the tip casing. The inlet flow is of axial direction and the outlet static pressure depends on the radius. The H-type grid used consists of 91 points in streamwise, 25 in pitchwise and 18 in spanwise direction. The results are plotted in the form of Mach number isolines in several planes along the span, see Fig. 4. Both methods give a very similar flow field structure. TVD MacCormack scheme captures the right running trailing edge shock at the hub better than the Ni's scheme, which maps better the left running trailing edge shock.

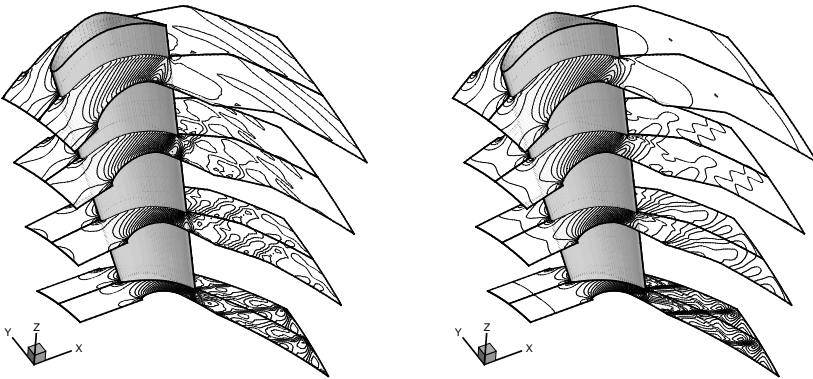


Fig. 4. (a) Stator, TVD MacCormack scheme, (b) Stator, Ni's scheme

The second cascade is the rotor cascade with highly twisted blades, typical for the LP steam turbine rotor cascades. Two different approaches have been applied. First, the rotor was considered to be in a non-rotating frame of reference. Relative flow field angles, two reference total quantities ϱ_0 , a_0 and ratios $\frac{\varrho_{rel,0}}{\varrho_0}$ and $\frac{a_{rel,0}}{a_0}$ at the inlet and static pressure distribution at the outlet section were prescribed. Because of the non-rotating frame of reference, this approach does not take into account body forces. H-type grid in this case consists of 81 points in streamwise, 25 in pitchwise and 18 in spanwise direction. Results obtained by both methods are in Fig. 5.a,b in the form of Mach number isolines. Again, a good agreement in the flow field structure can be observed. Slight dissimilarities are perceptible at the hub (the lowest cut in Fig. 5.a,b) and the shapes of isolines in the lowest but one cut in Fig. 5.a,b are different. Fig. 6 (x -axis is the radius and y -axis the Mach number) shows the radial distribution of Mach number along the inlet and outlet sections.

The latter approach uses a rotating frame of reference and the same inlet and outlet boundary conditions as the former. Body forces (centrifugal and Coriolis

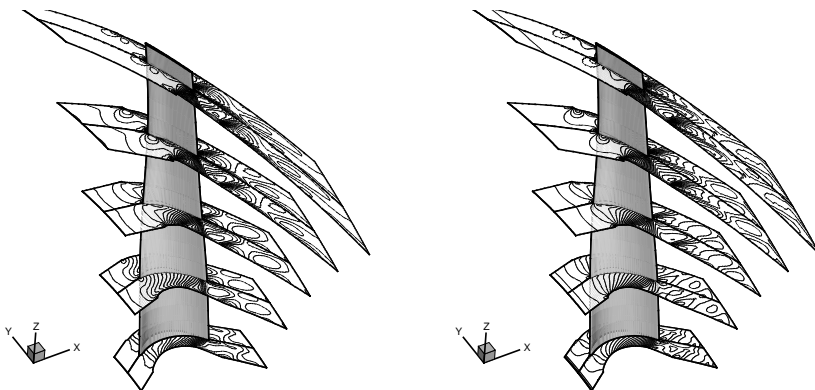


Fig. 5. (a) Rotor, TVD MacCormack scheme, (b) Rotor, Ni's scheme

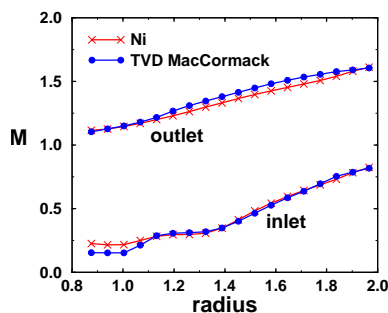


Fig. 6. Inlet and outlet Mach number distribution

forces) are now included. The next figures compare approaches mentioned on the basis of results computed by Ni's method. Considerable changes on the hub can be seen in Fig. 7.a,b, where isolines of the relative Mach number show stronger flow acceleration in the case without body forces as compared to the case with them. The velocity vectors plotted in a meridional cut in the middle between the blades detect the flow towards the hub in the case without body forces in contrast to the flow outwards the hub in the latter case, see Fig. 8. Finally, the relative Mach number as a function of the radius for both cases is plotted in Fig. 9, again a significant influence of body forces close to the hub is evident.

References

- [1] Ni R. H.: A multiple grid scheme for solving Euler equations. *AIAA J.* 20 (1981).
- [2] Causon D. M.: High resolution finite volume schemes and computational aerodynamics, *Notes on Numerical Fluid Mechanics*. vol. 24, Braunschweig, Vieweg, 1989, pp. 63–74.
- [3] Angot P., Fürst J., Kozel K.: TVD and ENO schemes for multidimensional steady an unsteady flows—a comparative analysis. *Proc. Finite Volumes for Complex Applica-*

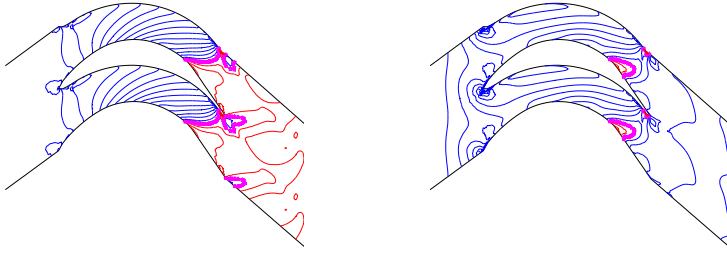


Fig. 7. (a) Without body forces, (b) With body forces

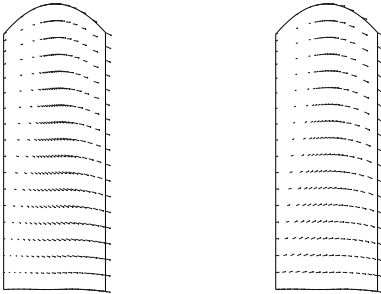


Fig. 8. Without (left) and with (right) body forces

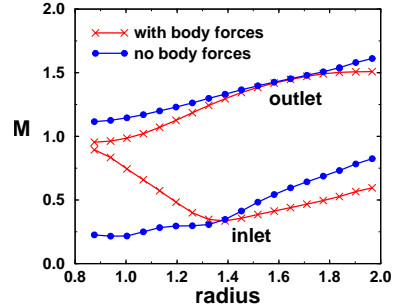


Fig. 9. Inlet and outlet Mach number

tions-Problems and Perspectives (F. Benkhaldoun, R. Vilsmeier Rouen, eds.). Hermes, 1996, pp. 283–290.

- [4] Fořt J., Fialová M., Fürst J., Horák M., Kozel K.: Numerical solution of several 2D and 3D internal flow problems. Proceedings of 15th International Conference on Numerical Methods in Fluid Dynamics, Monterey, USA (P. Kutler, J. Flores, J.-J. Chattot, eds.). Springer, Berlin, 1997, pp. 364–369.
- [5] Fořt J., Fürst J., Halama J., Kozel K.: Numerical solution of 3D inviscid transonic flows. Proceedings of The Seventh Asian Congress of Fluid Mechanics, (R. Narasimha, ed.). Madras, December, 1997, pp. 617–620.

Authors' addresses: J. Fořt, J. Fürst, J. Halama, K. Kozel, Department of Technical Mathematics, Faculty of Mechanical Engineering CTU Prague, Karlovo náměstí 13, CZ-121 35 Praha 2, Czech Republic, e-mail: fort@marian.fsik.cvut.cz, furst@marian.fsik.cvut.cz, halama@marian.fsik.cvut.cz, kozelk@fsik.cvut.cz.